Inlier Detection in Thermal Sensitive Images

E. Zadicario[1,2], N. Carmi[2], T. Ju[3] and D. Cohen-Or[1]

[1]Tel Aviv University, Israel
[2]InSightec Ltd, Israel
[3] Washington University in St. Louis, USA

Abstract

Image guidance of medical procedures may use thermal images to monitor a treatment. Analysis of the thermal images by the physician may be time consuming and confusing because the thermal image includes multiple outliers. We present a novel inlier detection method for thermal images that results in reliable thermal information to support medical decision making. Outliers in thermal images are particularly challenging to detect using conventional methods, because they are significantly more abundant than inliers and, like inliers, they may be temporally consistent. Our inlier detection method is physically-based: it is motivated by the fact that heat propagation in soft tissues can be modeled using the bio-heat equation. Pixels are classified as inliers only if the temperature pattern in a spatial and temporal neighborhood strongly correlates with the physical model. For improved robustness, the correlation process includes a 2D filter in the spatial domain and a 3D filter in both spatial and temporal domains. Experiments with real data have shown that our method produces results that agree with annotations provided by human experts even in outlier-laden images. Our results show inliers can be detected leaving true heat pixels for the physician to observe, while not overloading him with the need to analyze outliers. The technique has been integrated in a true clinical environment and is being used to aid physicians in analysis of thermal images

Categories and Subject Descriptors (according to ACM CCS): I.4 IMAGE PROCESSING AND COMPUTER VISION [Computer Graphics]: Image processing software—

1. Introduction

Digital imaging has grown to be an integrated tool in modern medicine. It enabled the development of Image Guided Therapy, a field that advanced medicine and significantly improved healthcare. An emerging method of therapy is by applying heat to a target tissue using High-Intensity Focused Ultrasound (HIFU). Above a threshold temperature a diseased tissue can be destroyed. The procedure is guided by Magnetic Resonance Imaging (MRI), which allows visualization of the tissue in a non-invasive manner and can also detect changes of temperature of the tissue. This combination of anatomical and thermal visualization provides a powerful monitor for surgeons to identify and treat tissue with real time feedback.

Unfortunately, due to limitations of MRI imaging, such as sensitivity to tissue movements (e.g., flow in vascular structures) and insensitivity to particular tissue types (e.g., bones), MRI thermal images are often abundant in regions where the measurement do not reflect a true temperature

rise. If undetected, these *outliers* could significantly degrade treatment outcome.

Removing outliers in MRI thermal images presents unique challenges. First, the amount of outlier pixels in the image usually significantly outweighs the *inliers*, which are pixels of focal point of energy and occupy a rather tiny fraction of the image data (less than 1%). Figure 1 shows an example of a target tissue in the brain. The temperature ranges from $37\,°C$ (normal body temperature) to $45\,°C$ and is colored in Figure 1 (b) from blue to red. Note that there are significant portions of the image away from the focal point of energy (green cross in Figure 1 (a)) that exhibit a high temperature. This is further illustrated in Figure 1 (c) where the masked pixels have a temperature above $41\,°C$. Since common statistical methods for outlier removal are effective when the ratio of inliers over outliers is significant, these methods cannot be applied to thermal images.

Additional challenges arise from the fact that true heating may occur anywhere in the image and is not limited to the planned target point. The outliers in thermal images, like

inliers, are temporally consistent. These properties make it difficult, if not impossible, to robustly detect outliers without any knowledge of the temperature behavior of inliers.

In this paper, we present a novel algorithm for inlier detection in thermal images that is based on modeling the temperature behavior of inliers. To the best of our knowledge, this is one of the first inlier detection methods that is based on a physical model. The premise of our approach is the fact that the spatial and temporal pattern of a heat source in a tissue is known and can be modeled.

The approach enables to automatically remove imaging artifacts and present to the physician the true heated areas. At the planned treatment point, the true dimensions of the heated area are shown. The approach will not ignore true heat even if it is away from the target, which has a lot of safety implications in a clinical situation.

Pixels in the thermal images are determined as inliers if the temperature behavior in a spatial and temporal neighborhood correlates well with the model. Inliers may be detected even if they are isolated and occupy an extremely small region (e.g., Figure 1 (d)). Our key technical contributions include the construction of two correlation filters based on the spatial and temporal model of heat distribution, and an inlier mask that combines the filters with spatial clustering. Our method has been integrated in a clinical system and we demonstrate its effectiveness on several real-world data.

a) Brain anatomy b) Thermal image

c) Thermal threshold mask d) Physical model mask
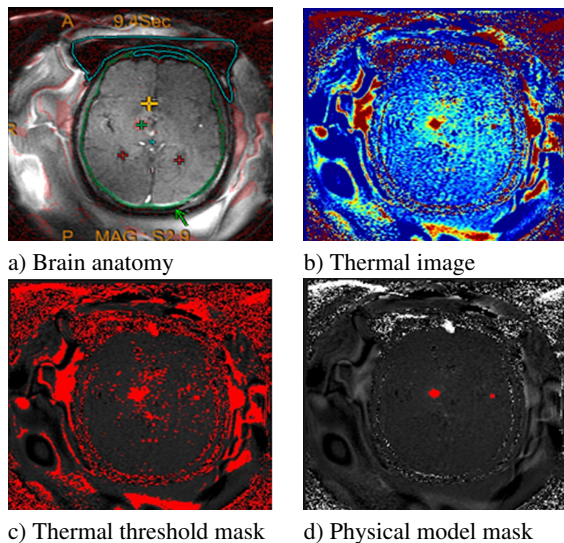
Figure 1: *An example of thermal ablation of the brain shows the anatomy and its surroundings (a) next to the thermal image where each pixel is colored by the measured temperature value (b). A simple denoising mask detects pixels in which the temperature crosses $41\,^\circ$C degrees (c) whereas the model-based detection mask (d) clearly shows areas where true heat has been measured while ignoring outliers.*

2. Related Work

Inlier and outlier detection techniques have been studied in the community of statistics and data mining for decades [Gru69]. The motivation is to detect anomalies in the data [EAP*02, CBK09] and to remove misleading samples from the data for further analysis [LSJ04]. In measurement of physical systems, excluding outliers is commonly applied to enhance further analysis. Subjective exercise has shown that excluding the distorted samples retrieves a more reliable modeling of the data [HA04].

Statistical methods assume normal or other predetermined distribution of the data points [Ros03] to identify outliers. RANSAC is a most common technique that uses statistical methods for the detection of outliers [FB81]. By iterative random selection of subset of data points it retrieves those that best fit a parametric model and excludes the outliers. It is most effective when the portion of inliers is significant and it provides a tradeoff between the number of iterations and an acceptable solution. To accelerate the performance, locally optimized versions have been suggested [CMK03]. Increasing the number of inliers near the suggested optimum speeds up the RANSAC procedure by allowing its earlier termination and leads to results of higher quality. The use of statistical methods has the advantage of being unsupervised, detecting outliers without prior knowledge of a predefined model. However, it is inefficient if the portion of inliers is low.

Model-based outlier detection has been suggested in situations where the nature of the measured data is known. These are supervised methods, where prior knowledge of the context of the data can help in outlier detection. For example, when sampling velocity and trajectories, outliers can be detected based on the context of the sampled data [YPSC10]. Such models screen outliers based on statistics and context aware analysis. A context aware physical model leads to detection methods that are robust even in situations where the ratio of inliers is low.

Medical image is used to visualize a measurement of tissue property or physical phenomena (e.g. CT, MRI, US, X-Ray) [Doi05] which may include outliers. Segmentation and automatic detection of abnormalities, such as brain tumor delineation, require robust estimation and outlier detection mechanisms [FVPT12]. A parabolic model has been used to detect outliers when tracking moving surface of the open brain in surgical procedures [RV13]. Segmentation of arteries in ultrasound images has also been improved by using a combined approach of edge detection technique and RANSAC outlier detection to yield a robust semi-automatic segmentation [RCS*11]. Detection of outliers is used to improve segmentation of tissue structures [LMY07, HM09], to support a robust sampling of tissue properties [MTGM*08] and to aid in diagnosis of clinical anomalies [PBHG04, VLMV*01]. The use of a known physical model can significantly enhance outliers detection.

We are interested in medical treatments that apply heat to destroy tissue using ultrasound, while measuring the temperature using MRI [CSH*92, JM14, HVC*97]. The thermal imaging is used to monitor the heating of the tissue, to overcome tissue variability and to insure targeting alignment [VSJ*00]. The effects of heat on living tissue and its distribution profiles have been mapped and validated with the solving of the bio-heat transfer equation [HCH01, CP02, Nyb88, SYLK07]. These models have been tested and validated in the living tissue [CP02]. The availability of a known physical model of the bio-heat transfer can be applied to enhance the confidence in thermal images by ruling out misleading information which does not reflect true thermal measurement.

3. Background

During HIFU treatment, ultrasound energy is applied to heat tissue in the brain through an intact skull. The ultrasound energy traverses through the scalp, the skull and healthy brain tissue to focus the heat at the desired target location. Figure 2 depicts a diagram of the ultrasonic rays traversing through the tissue to the target and a typical thermal image. When the energy is being delivered, there is a need to monitor the thermal rise of the intended target tissue. Equally important is to observe that there is no unintended heating anywhere else in the brain which may occur due to local tissue characteristics (e.g., calcifications).

a) Ultrasonic rays   b) Thermal image
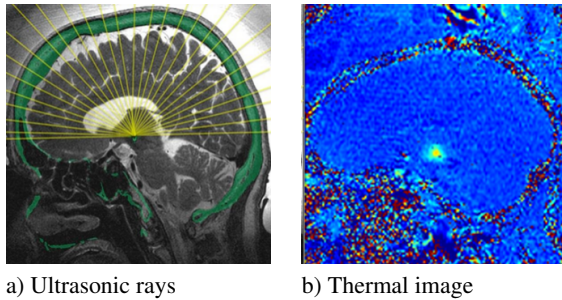
Figure 2: *Non-invasive ultrasound system for brain treatment. (a) The ultrasonic rays traversing through the tissue to the intended target and (b) a typical thermal image.*

Thermal sensitive imaging allows real time feedback to control medical procedures of tissue ablation. MRI scans the target and its surrounding area to generate thermal images. Current MRI technology is limited in temporal resolution when acquiring 3D volumes. To overcome this we use two dimensional scans that are taken at a temporal resolution that can span from one to five seconds. The thermal data set for each energy deposition cycle includes a planar image, going through the intended focal plane, and mapping its surroundings at predetermined time points. The images are stacked together over the time domain to create a three dimensional data set.
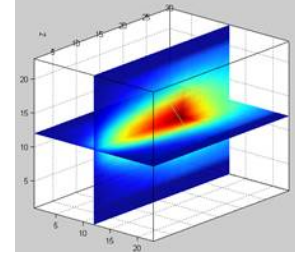
Figure 3: *A three dimensional template to estimate the spatial and temporal heat distribution model.*

The physical measurement is very sensitive and may be imperfect due to tissue movement, noise and erroneous measurement. As a result the set of thermal measurements often includes some misleading outliers. It is essential to detect the outliers in the thermal measurement to report the true thermal effect and support reliable clinical decision making.

While the focal area of heating can be easily noticed in thermal images, it is challenging to determine the actual thermal rise in other areas of the brain and the scalp. The difficulty comes from several aspects. The first is that unintended heat may occur anywhere, thus the entire image needs to be analyzed for heating. In addition, the actual heated region may be tiny, so its impact on any statistical analysis (e.g., median) is negligible and spatial filtering may overlook true heating.

4. Method

4.1. Overview

Our approach utilizes the fact that physical phenomena of heat, its absorption in the tissue, and the dissipation of heat in surrounding tissue is well modeled by the bio-heat transfer equation. The model describes the spatial distribution of temperature in the tissue and its temporal behavior over time. When we apply this criteria to outlier detection we can detect outliers that do not correspond to a physically feasible temperature pattern.

Using the heat transfer properties of the tissue, we first build a temperature curve that describes the temperature distributed in the volume as a function of its distance from the heat source. Based on the known temperature curves we construct a 3D template that estimates the temperature in a 2D temperature spatial distribution and along the time domain (see Figure 3). The template is calculated with respect to the specific heat pattern that is applied (see Section 4.2).

Given the bio-heat template and the sampled thermal images over time, we can quantify the correlation between the sampled data and the model. This is performed by combining two correlation scores. First, we know that for every pixel that reflects significant heat the neighboring pixels
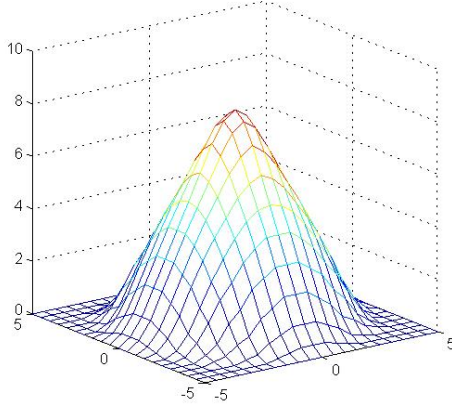
Figure 4: *A 2D correlation template used as the spatial filter.*

Figure 5: *Temperature profile over time for pixels around the heat focal point.*

must have similar thermal rise since heat naturally dissipates to its surroundings. We use the bio-heat transfer model to create a 2D spatial filter that scores each pixel against the expected heat dissipation across the tissue (Section 4.3). Second, to obtain additional confidence we use the 3D bio-heat temporal model and calculate a 3D correlation score at each pixel using its 3D neighborhood in the time dependent stack of thermal images (Section 4.4). Inliers are then detected as clusters of pixels with high correlation scores (Section 4.5).

4.2. Bio-Heat Model Preprocessing

The distribution model of the heat in the tissue has two components. The first is a simulation of the focused acoustic ultrasound field and how its pressure field translates to heat. The second is the bio-heat equation. It is used to describe the dissipation of heat in the tissue and its propagation over time. The general bio-heat equation is give by:
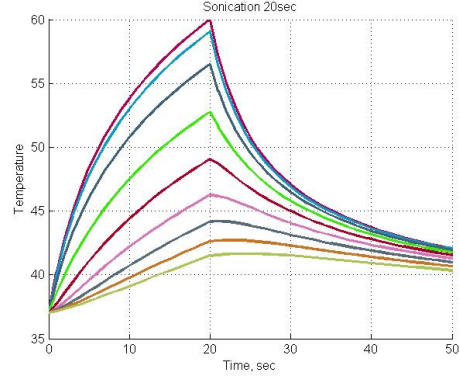
$$\rho_t c_t \frac{\partial T}{\partial t} + W_b C_b (T - T_a) = k \frac{\partial^2 T}{\partial x^2} + Q \qquad (1)$$

where ρ_t is the density, c_t is the specific heat capacity of the tissue, T is the tissue temperature, t is the time, W_b is the perfusion rate, C_b is the specific heat capacity of blood, T_a is the supplying arterial blood temperature, k is the thermal conductivity of tissue, Q is the heat deposition source term due to the acoustic field, and x is the distance from the heat source. Solving this equation for the specific tissue profile gives us the spatial distribution model in the tissue.

4.3. Spatial Correlation Filter

With a model of the temperature distribution around a heat source we can detect which areas in the thermal image correspond to the expected behavior. Figure 4 shows a typical temperature distribution around the focal point.

We use the two dimensional cross correlation function to compare each section in the sampled image. For each pixel we get a correlation score that is defined by the following mean square error function:

$$r_{2D} = \frac{\sum\limits_{i \in M} \sum\limits_{j \in N} (D_{ij} - T_{ij})^2}{\sum\limits_{i \in M} \sum\limits_{j \in N} (\max(T) - T_{ij})^2} \qquad (2)$$

Here the value r_{2D} is the correlation error, T is our template model patch of size $M \times N$, and D is a corresponding patch of the same size from the thermal image. The correlation score is $1 - r_{2D}$. Examining the result, areas with high correlation (low mean squared error values) point to the areas matching the spatial heating behavior.

4.4. Temporal Correlation Filter

The physical model we are using describes spatial as well as temporal heat distribution of heat in the tissue. The sampled thermal images are also taken at different time points along the heating process. The correlation between the model and the sampled data in the time domain adds robustness to the outlier detection method.

Using the bio-heat model we estimate heat profile over time for the focal heated point and for its surroundings depending on the distance from the focal heat. Figure 5 shows an example of the temperature evolution when the energy is applied for 20 seconds. The temperature rises through the first 20 seconds and then the tissue cools down when the energy deposition is stopped. The peak temperature is at the focal point of the heat and is shown in the hottest profile. The other profiles reflect the temperature history for neighboring pixels around the focal point. It can be seen that the heat profile over time depends on the distance of the pixel from the focal point.

With this spatial and temporal information we construct a three dimensional template modeling the heat dissipation

over time. Figure 3 shows an example of such a template. Similarly, we have thermal images that are taken at multiple discrete time points along the heating cycle, typically 6-10 images over 20-30 seconds.

The template is used to detect the potential candidate inlier pixels by scoring the correlation with the model in the time domain. For this correlation scoring we use a three dimensional correlation error given by:

$$r_{3D} = \frac{1}{MN} \sum_{i \in M} \sum_{j \in N} \frac{\sum_t [(D_{ijt} - \overline{D}) - (T_{ijt} - \overline{T})]^2}{\sum_{t \in T} (T_{ijt} - \overline{T})^2} \quad (3)$$

where T is a 3D template, and D is a sub-volume from the sampled data set. Both have the size of $M \times N$ in the 2D spatial domain and t samples in the third time domain. $\overline{T}$ and $\overline{D}$ are the mean values of the 3D template and sampled data set, respectively. The temporal correlation score is $(1 - r_{3D})$.

4.5. Inlier Detection Mask

The final step takes the 2D spatial correlation analysis and the 3D spatial-temporal correlation scores to generate a physical inlier mask. We combine the scores from both parts to obtain the most robust results. In creating the mask we want to emphasize again the fact that a valid heat measurement tends to have a specific spatial distribution. In particular, we expect that all pixels in a valid heated region will have some correlation with the heat model and some pixel in the region must have a high correlation value.

As a first step we combine the 2D and 3D correlation scores for each pixel into a unified correlation map. We define a combined correlation score by multiplying the two correlation values,

$$CorrMapValue(i, j) = r_{2D}(i, j) \times r_{3D}(i, j) \quad (4)$$

The score is further normalized by the maximal value in the current image stack. Thus, we get the *Normalize Correlation Map* by

$$NormCorrMap(i, j) = \frac{CorrMapValue(i, j)}{\max(CorrMapValue)} \quad (5)$$

To identify the inliers using the *Normalize Correlation Map*, we apply physical concepts that are valid for our model. First we filter out all pixels whose values of *Normalized Correlation Map* are below a predefined *Low Correlation Threshold*. The remaining pixels are potentially valid inliers.

Next, we know from our model that valid inliers cannot be isolated pixels. We therefore apply a clustering algorithm within the potentially valid pixels to generate inlier clusters. The brute force clustering applies high threshold to the thermal map. Arround each pixel we create a mask based on dilation technique until a low threshold value is reached. We keep only clusters that contain some pixel with significantly

high correlation, that is, its *Normalized Correlation Map* value is higher than some user-given *Cluster High Threshold*. This final step marks the pixels that are considered as inliers and make up the *Inlier Detection Mask*.

The threshold values were established by a clinical expert using 50 training data sets. The expert was asked to mark the valid heated area on the thermal image. An *Inlier Detection Mask* was calculated for each data set. The *Low Correlation Threshold* and the *Cluster High Threshold* were then modified until they provide maximal detection of outliers while minimizing the cases where valid heat is classified as an outlier (i.e., a false positive). This is motivated by the fact that, due to safety implications associated with missed heating, we cannot allow cases of false positive but may tolerate some true negative.
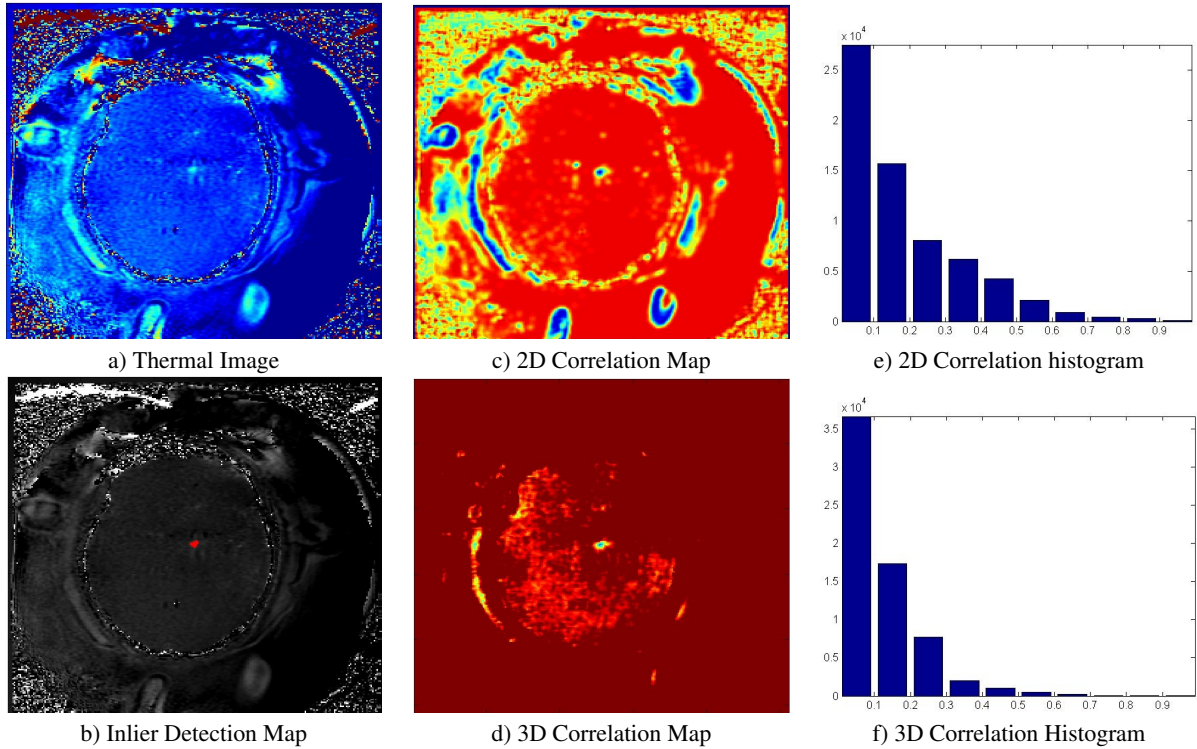
Figure 6 shows an example of how various thresholds impact the inlier mask. It can be seen how lower thresholds include inliers which were rejected by the clinical expert. The final thresholds were set to 0.3 and 0.6 for the *Low correlation Threshold* and *Cluster High Threshold*, respectively. These values were kept consistent throughout the testing of the data sets. The rationale for setting these thresholds is based on the need to minimize the false positive. In such a case true heat will be masked from the physician and may lead to improper clinical decision.

a) Thermal Image   b) Inlier Mask 0.4 0.1

c) Inlier Mask 0.5 0.2   d) Inlier Mask 0.6 0.3
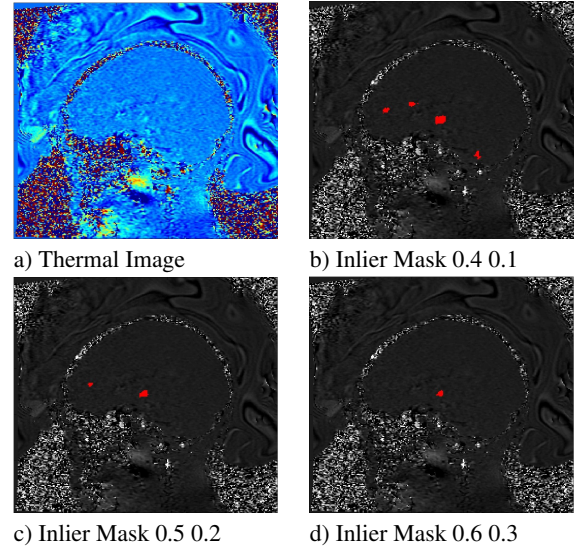
Figure 6: *Inlier Detection Masks with various thresholds.*

5. Results

The outlier detection method, based on a physical model, has been integrated in a clinical system that is being used for thermal ablation using focused ultrasound. We collected 50 data sets of thermal scans taken during a thermal ablation process of the brain. These data sets were different from

| a) Thermal Image | c) 2D Correlation Map | e) 2D Correlation histogram |
| b) Inlier Detection Map | d) 3D Correlation Map | f) 3D Correlation Histogram |

Figure 7: *An example of inlier detection results. The original thermal image (a) next to the Inlier Detection Mask (b) where inlier pixels are marked in red. The 2D Correlation Map (c), the 3D Correlation Map (d), and the respective histograms for the scores (e) and (f).*

the ones used for the training set from which our threshold values were determined (see above).

In all the cases that we are studying, the area of the true heat occupies a tiny portion of the thermal image. Figure 7 shows an example case which is typical of the tested cases. Figures 7 (a) and (b) show the original thermal image and the *Inlier Detection Mask*, respectively. In this case only a negligible portion of less than 1% of all pixels are inliers. This is the main reason why a physical model is essential to support a robust outlier detection method. Any statistical method would be very limited in picking up such a small subset of inliers.

This example demonstrates the importance of the two correlation maps. The combination of spatial 2D correlation and 3D temporal correlation is critical to have a robust algorithm to confirm that inlier pixels comply with both temporal and spatial behavior of the physical model. Figures 7 (c) and (d) show the 2D correlation and the 3D correlation maps, respectively. Figures 7 (e) and (f) show histograms of the 2D correlation and 3D correlation, respectively. In each bin we present the number of pixels with the corresponding correlation value. It can be seen that the maps are very different and that only the combination reflects a robust view of the inliers

in the thermal image. The combination of the two filters is the outcome mask shown in Inlier Detection Map (b).

The example in Figure 8 shows an additional benefit of using a physical based algorithm. Although we know where to expect the focal heating to be, one cannot exclude situations in which there is valid heat away from the target area. This is due to the nature of the tissue and the way the ultrasound is applied. It is therefore important to validate that such distant heating is detected by the algorithm. Such event is rather rare, so there was no true case of unplanned heat-

| a) Thermal Image | b) Inlier Mask |
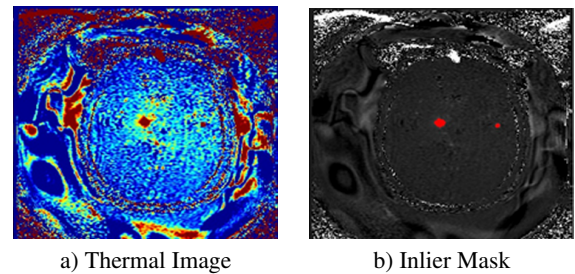
Figure 8: *An example of detection of distant inlier.*

| a) Thermal Image | b) Threshold Mask | c) Inlier Detection Mask |
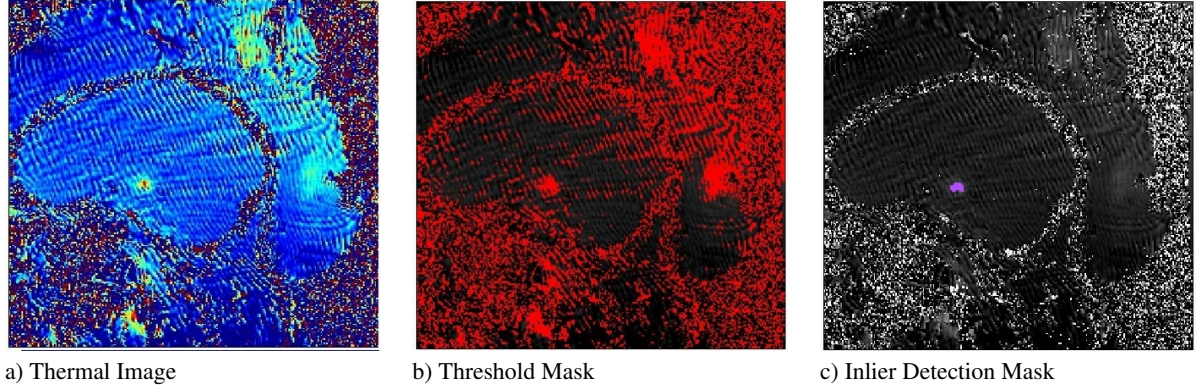
Figure 9: *An example of inlier detection results. The original thermal image (a) next to the threshold mask (b) and the Inlier Detection mask (c) which shows a score of 0.95.*

ing in our collection of clinical data sets. To test this we had to use a simulated data that mimics this situation. To simulate distant heating we used a small patch of a true heating, scaled it down and superimposed it in a distant location from the target. Without being aware of the simulated data set, it was analyzed by a clinical expert who marked this to be valid heating. It can be seen in Figure 8 (b) that the distant area is also marked as an inlier.

In addition to the expert validation, we compared our physically based *Inlier Detection Mask* to a naive *Threshold Detection Mask*, which is set to be 41 °C degrees. The comparison is done in two steps. First, we compare the number of suggested inliers in each mask. The number of inliers in the *Inlier Detection Mask* is noted by N_{Inlier}, while the number of inliers in the *Threshold Detection Mask* is noted by $N_{Threshold}$. We expect N_{Inlier} to be significantly different and smaller than $N_{Threshold}$. Thus we define the *Inlier Detection Score* as the (relative) difference in the two numbers,

$$InlierDetectionScore = \frac{|N_{Threshold} - N_{Inlier}|}{N_{Threshold}} \quad (6)$$

A score close to one implies a large difference in the inlier numbers. Next, we asked the clinical expert to review whether there are any true inliers that were masked out in the *Inlier Detection Mask*. These cases were considered as failure, and we set the *Inlier Detection Score* of these images to zero.

Figure 9 shows an example of one of the data sets – the original thermal image (a), the *Threshold Detection Mask* (b) and the *Inlier Detection Mask* (c). In this case the *Inlier Detection Score* is 0.95. The average score in our 50 data sets was 0.81 with the best score being 0.97 and the lowest 0.42. There were no cases that failed due to unmasked pixels which were classified by the clinical expert as inliers.

The run-time performance of the algorithm depends primarily on the actual data set. For example, the longer the heating process, the more thermal data there is to analyze. The wider the field of view of interest, the larger the area that needs to be analyzed. In general we used this approach for analyzing heating process of 20-30 seconds and field of view of 256×256 pixels in each frame. Under these settings the run-time to obtain the *Inlier Detection Mask* ranged from 200 msec to 1100 msec on a single core PC running Windows XP.

6. Conclusions

Image guided medical procedures demand reliable visualization to support clinical decision making. Thermal images are used to monitor surgeries performed with MRI-guided focused ultrasound. The nature of the imaging technology results in outliers that could significantly impact decision making. Outliers in these images are particularly challenging to detect using existing methods due to their sheer quantity and temporal consistency. To this end, we present a novel, physically based outlier detection method. We overcome the challenge using a known physical model of heat propagation. Pixels are classified as inliers if the measurement in a spatial and temporal neighborhood correlates with the physical model. Experiments with real world data show that our method is capable of identifying small, isolated hot spots that agree with expert markings in real-world, outlier-laden images. While the current work focuses on thermal images of the brain, the method can be applied to various other tissues and organs by using appropriate parameters for the heat model. In the future, we would like to explore means that can further accelerate the computation, such as using hierarchical filters or parallelizing the correlation using graphics hardware.

References

[CBK09] CHANDOLA V., BANERJEE A., KUMAR V.: Anomaly detection: A survey. *ACM Computing Surveys (CSUR) 41*, 3 (2009), 15.

[CMK03] CHUM O., MATAS J., KITTLER J.: Locally optimized ransac. In *Pattern Recognition*. Springer, 2003, pp. 236–243.

[CP02] CHENG H.-L. M., PLEWES D. B.: Tissue thermal conductivity by magnetic resonance thermometry and focused ultrasound heating. *Journal of Magnetic Resonance Imaging 16*, 5 (2002), 598–609.

[CSH*92] CLINE H. E., SCHENCK J. F., HYNYNEN K., WATKINS R. D., SOUZA S. P., JOLESZ F. A.: MR-guided focused ultrasound surgery. *Journal of computer assisted tomography 16*, 6 (1992), 956–965.

[Doi05] DOI K.: Current status and future potential of computer-aided diagnosis in medical imaging. *British Journal of Radiology 78*, 1 (2005), 3–19.

[EAP*02] ESKIN E., ARNOLD A., PRERAU M., PORTNOY L., STOLFO S.: A geometric framework for unsupervised anomaly detection. In *Applications of data mining in computer security*. Springer, 2002, pp. 77–101.

[FB81] FISCHLER M. A., BOLLES R. C.: Random sample consensus: a paradigm for model fitting with applications to image analysis and automated cartography. *Communications of the ACM 24*, 6 (1981), 381–395.

[FVPT12] FRITSCH V., VAROQUAUX G., POLINE J.-B., THIRION B.: Non-parametric density modeling and outlier-detection in medical imaging datasets. In *Machine Learning in Medical Imaging*. Springer, 2012, pp. 210–217.

[Gru69] GRUBBS F. E.: Procedures for detecting outlying observations in samples. *Technometrics 11*, 1 (1969), 1–21.

[HA04] HODGE V. J., AUSTIN J.: A survey of outlier detection methodologies. *Artificial Intelligence Review 22*, 2 (2004), 85–126.

[HCH01] HALLAJ I. M., CLEVELAND R. O., HYNYNEN K.: Simulations of the thermo-acoustic lens effect during focused ultrasound surgery. *The Journal of the Acoustical Society of America 109*, 5 (2001), 2245–2253.

[HM09] HEIMANN T., MEINZER H.-P.: Statistical shape models for 3d medical image segmentation: A review. *Medical image analysis 13*, 4 (2009), 543–563.

[HVC*97] HYNYNEN K., VYKHODTSEVA N. I., CHUNG A. H., SORRENTINO V., COLUCCI V., JOLESZ F. A.: Thermal effects of focused ultrasound on the brain: determination with MR imaging. *Radiology 204*, 1 (1997), 247–253.

[JM14] JOLESZ F. A., MCDANNOLD N. J.: Magnetic resonance–guided focused ultrasound: A new technology for clinical neurosciences. *Neurologic clinics 32*, 1 (2014), 253–269.

[LMY07] LEKADIR K., MERRIFIELD R., YANG G.-Z.: Outlier detection and handling for robust 3-d active shape models search. *Medical Imaging, IEEE Transactions on 26*, 2 (2007), 212–222.

[LSJ04] LIU H., SHAH S., JIANG W.: On-line outlier detection and data cleaning. *Computers & chemical engineering 28*, 9 (2004), 1635–1647.

[MTGM*08] MANJÓN J. V., TOHKA J., GARCÍA-MARTÍ G., CARBONELL-CABALLERO J., LULL J. J., MARTÍ-BONMATÍ L., ROBLES M.: Robust MRI brain tissue parameter estimation by multistage outlier rejection. *Magnetic Resonance in Medicine 59*, 4 (2008), 866–873.

[Nyb88] NYBORG W. L.: Solutions of the bio-heat transfer equation. *Physics in medicine and biology 33*, 7 (1988), 785.

[PBHG04] PRASTAWA M., BULLITT E., HO S., GERIG G.: A brain tumor segmentation framework based on outlier detection. *Medical Image Analysis 8*, 3 (2004), 275–283.

[RCS*11] ROCHA R., CAMPILHO A., SILVA J., AZEVEDO E., SANTOS R.: Segmentation of ultrasound images of the carotid using ransac and cubic splines. *Computer methods and programs in biomedicine 101*, 1 (2011), 94–106.

[Ros03] ROSS S. M.: Peirce's criterion for the elimination of suspect experimental data. *Journal of Engineering Technology 20*, 2 (2003), 38–41.

[RV13] REFAEL VIVANTI OFRI SADOWSKY M. S. L. J.: Brain tissue deformation tracking with a paraboloid model for outlier detection. In *CARS2013*. 2013.

[SYLK07] SHIH T.-C., YUAN P., LIN W.-L., KOU H.-S.: Analytical analysis of the pennes bioheat transfer equation with sinusoidal heat flux condition on skin surface. *Medical Engineering & Physics 29*, 9 (2007), 946–953.

[VLMV*01] VAN LEEMPUT K., MAES F., VANDERMEULEN D., COLCHESTER A., SUETENS P.: Automated segmentation of multiple sclerosis lesions by model outlier detection. *Medical Imaging, IEEE Transactions on 20*, 8 (2001), 677–688.

[VSJ*00] VYKHODTSEVA N., SORRENTINO V., JOLESZ F. A., BRONSON R. T., HYNYNEN K.: MRI detection of the thermal effects of focused ultrasound on the brain. *Ultrasound in medicine & biology 26*, 5 (2000), 871–880.

[YPSC10] YAN Z., PARENT C., SPACCAPIETRA S., CHAKRABORTY D.: A hybrid model and computing platform for spatio-semantic trajectories. In *The Semantic Web: Research and Applications*. Springer, 2010, pp. 60–75.